Propagation of second sound near T_λ

D. R. Swanson, T. C. P. Chui, and J. A. Lipa
Department of Physics, Stanford University, Stanford, California 94305
(Received 30 September 1991; revised manuscript received 19 May 1992)

Superfluid hydrodynamics for second sound, expanded to first order in $\nabla\rho_s$ and including second-sound damping and finite-amplitude effects, are cast into a boundary-value-problem format, suitable for calculating the resonant frequency in a second-sound cavity operating near the λ point. This model is applied to the data of Marek, Lipa, and Philips, which showed deviations from a simpler model in the region close to the transition. We find that our model by itself cannot explain the deviations, but if a shift in the estimated location of T_λ is included, a significant improvement can be obtained. The critical exponent ζ, describing the divergence of ρ_s, was found to be $\zeta=0.6708\pm0.0004$, in good agreement with the renormalization-group prediction 0.672 ± 0.002. The range for the reduced temperature parameter was extended to $\varepsilon=2\times10^{-7}$, substantially closer to the transition than in the previous analysis of this data. The shift in T_λ can be considered acceptable if the data very near T_λ are reinterpreted. The effect of the $\nabla\rho_s$ term is shown to be important for $\varepsilon<10^{-6}$.

I. INTRODUCTION

With the development of subnanokelvin thermometry,[1] the measurement of thermodynamic properties near the λ transition in ^{4}He is now limited primarily by the dependence of the transition temperature, T_λ, on hydrostatic pressure. For sample sizes of a few mm, this limit[2] is of the order 10^{-7} on the reduced temperature scale $\varepsilon\equiv|1-T/T_\lambda|$. Further from the transition, the gravitational effect is observable as a distortion of the data which, in many cases, is small and easily calculable, but for ε below the limit, the effect rapidly dominates. With smaller samples, finite-size effects soon become noticeable. Recent measurements[3] by Marek, Lipa, and Philips (MLP) of the second-sound frequency in a cavity resonator of 1.3-cm height have been made very close to T_λ, with a significant amount of data in the region affected by gravity. The MLP data, approaching T_λ to within 10^{-7} K, represent a stringent test of the renormalization-group (RG) prediction[4] for the critical exponent ζ, describing the divergence of the superfluid density ρ_s near T_λ. However, MLP obtained reasonable agreement with their model only over the limited range $3\times10^{-6}<\varepsilon<10^{-3}$. Below $\varepsilon\sim3\times10^{-6}$, the experimental results displayed deviations of several percent (see Fig. 1) from a time-of-flight model describing the effect of gravity on second-sound propagation near the transition. Since the results of MLP represent one of the few cases where significant departures from theory have been observed in the asymptotic region, it is important to explore the extent to which various factors neglected in their analysis may be contributing. It is not clear whether the deviations below $\varepsilon\sim3\times10^{-6}$ are an artifact of the time-of-flight model, a true departure from theory, or due to systematic errors in the experiment.

In this paper we attempt to clarify the situation by developing a more refined treatment of the gravitational effect and exploring the effects of damping and finite amplitude. We also investigate the effects of experimental uncertainties in the location of T_λ by including in the least-squares-fitting function, a parameter ΔT_λ, which shifts the temperature scale of the raw data. Altogether, five new effects are considered: the T_λ shift, finite amplitudes, damping, boundary effects, and an expansion to first order of $\nabla\rho_s$ in the differential equation describing second sound. Most significant were the shift in T_λ and the $\nabla\rho_s$ term in the differential equation. Our analysis of the second-sound problem is developed from a boundary-value perspective in which the second-sound frequency arises out of the resonant solution to the differential equation with matched boundary conditions. The implicit pressure dependence of the standard "gravity-free" model is incorporated through the variation of the local superfluid density with height. In con-

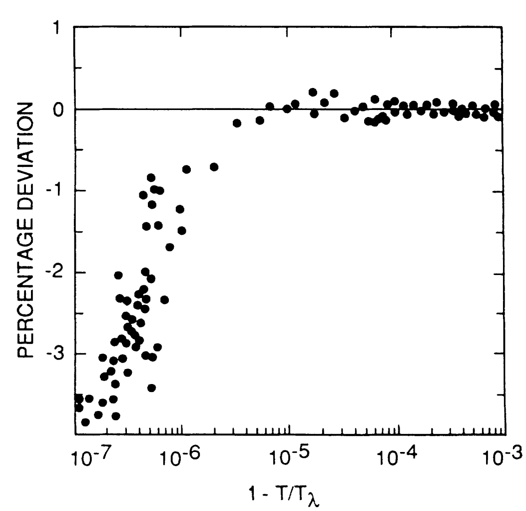

FIG. 1. Deviations of second-sound frequency from the time-of-flight model of MLP.

trast, the time-of-flight model described by MLP allows for the effect of gravity by summing the local second-sound velocity over the height of the resonator. To first order, the boundary-value approach and the time-of-flight method are equivalent, with the exception of the boundary effects neglected in the time-of-flight model. However, the boundary-value approach is more powerful in that it can be extended to include higher-order effects, i.e., our model treats the variation in the superfluid density to second order by including a term proportional to $\nabla\rho_s$. A further benefit of the boundary-value approach is that the wave-function solution gives complete information on the temperature profile of the second sound in the resonator, particularly the second-sound amplitude as a function of the input driving power.

By use of the boundary-value model and including a T_λ shift, we obtain the best-fit result $\zeta=0.6708\pm0.0004$, over the range $2\times10^{-7}<\varepsilon<10^{-3}$ where the uncertainty is estimated at one standard deviation. Our result agrees well with the RG prediction[4] $\zeta=0.672\pm0.002$ and the best previous result[5] $\zeta=0.6716\pm0.0004$, fit over the range $2\times10^{-5}<\varepsilon<10^{-2}$. The best-fit result for the T_λ shift is several times larger than the uncertainty quoted by MLP. This can be understood only by re-examining the criteria used in determining the location of the λ point. Our model indicates that there is a much sharper dropoff in the second-sound amplitude very near T_λ than originally assumed. This would lead to a bias in T_λ of about the right magnitude. Both the shift in T_λ and the boundary model are required to obtain a good fit over the entire data range. By only shifting T_λ and neglecting the effects in the boundary-value model, we are able to extend the range of agreement by about a factor of 3 closer to T_λ (to $\varepsilon\sim10^{-6}$). With the boundary model alone and no T_λ shift, the deviations are slightly worse than the MLP model.[6] It now appears that the MLP result $\zeta=0.6740\pm0.0005$ over the range $10^{-6}<\varepsilon<10^{-3}$ should be discarded due to the limitations of the approach then used.

In Sec. II, we set up a problem using the two-fluid model in its ideal nondissipative form and discuss the numerical techniques used to solve the differential equation. Examples of the resonant wave function are displayed for various cell temperatures. In Sec. III, we describe extensions to the basic boundary-value problem in Sec. II to include second-order effects, namely, second-sound damping and finite amplitudes. An order-of-magnitude estimate is made for the shift in resonant frequency due to both damping and finite-amplitude effects. Section IV contains the results and discussion of several least-squares fits to the MLP data, applying different combinations of the effects in the boundary-value model and the T_λ shift. An examination is made of various approximations used which may affect the accuracy of our model. We briefly summarize and make suggestions for future experiments in Sec. V.

II. BOUNDARY-VALUE PROBLEM IN THE LOW-AMPLITUDE LIMIT

The derivation of the differential equation for second sound from Khalatnikov's theory of two-fluid hydrodynamics[7] is straightforward. In the absence of dissipation the linearized equation, for small variations total in the entropy S, is

$$\partial^2S(z,t)/\partial t^2=u_{\mathrm{II}}^2\nabla^2S(z,t)\ , \tag{1}$$

where u_{II}^2 is the velocity of second sound:

$$u_{\mathrm{II}}^2=\rho_sTS^2/\rho_nC_p\ . \tag{2}$$

Here ρ_n is the normal fluid density and C_p is the specific heat at constant pressure. Near T_λ the superfluid density can be expressed in the form[5]

$$\rho_s=k\varepsilon^{\zeta}(1+a_0\varepsilon^{\Delta})\ ,\quad k=k_0(1+k_1\varepsilon)\ , \tag{3}$$

where the critical exponents ζ and Δ are determined by renormalization-group techniques[4] or from fitting (along with the coefficients k_0, k_1, and a_0), to experimental results.[5] The specific heat just below T_λ is written as

$$C_p=(A'/\alpha')\varepsilon^{-\alpha'}[1+D'\varepsilon^{\Delta}]+B'\ , \tag{4}$$

where α', A', D', and B' are similarly determined.[8] The expansion of the total entropy in terms of the reduced temperature near T_λ is taken from Ref. 5. This entropy expansion is obtained by integrating a specific-heat function slightly different from (4). This is adequate for the work described here as the entropy asymptotically approaches a constant value at T_λ to order $\varepsilon^{1-\alpha}$.

The effect of hydrostatic pressure on T_λ in the Earth's gravitational field ($dT_\lambda/dz=1.273\times10^{-6}$K/cm) induces a nonlinearity in the superfluid through the dependence of the fluid parameters [Eqs. (2)–(4)] on the reduced temperature:

$$d\varepsilon/dz=(1-\varepsilon)/T_\lambda\times dT_\lambda/dz\ . \tag{5}$$

For clarity we note that the reduced temperature varies along the height of the cell while the absolute temperature is uniform throughout the cell. In the MLP resonator, the reduced temperature increases by 7.6×10^{-7} from bottom to top. This has the implication that the resonant frequency is derived from an average of the fluid properties in the cell. For $\varepsilon<10^{-6}$, where this gravitational effect becomes significant, we make use of the locally defined $\varepsilon(z)$ and from (2)–(4), the locally defined second-sound velocity $u_{\mathrm{II}}(z)$. This induces an implicit nonlinearity in the differential equation (1) which increases rapidly at small ε. For the small sample height used by MLP, we can safely neglect the pressure dependence of the parameters in (3) and (4). All the values of ε quoted in this paper refer to the local value at the bottom of the cell.

Near T_λ, other more explicit nonlinear effects, which were neglected in the derivation of (1), may also become significant. These include terms involving powers of $\nabla\rho_s$, finite-amplitude effects, and second-sound damping. By including terms up to first order in $\nabla\rho_s$, the differential equation becomes[9]

$$\partial^2T_1(z,t)/\partial t^2=u_{\mathrm{II}}^2(z)[\nabla^2T_1(z,t)+\nabla\rho_s(z)\nabla T_1(z,t)/\rho_s]\ , \tag{6}$$

where T_1 is the amplitude of the second-sound wave. The differential equation is now expressed in terms of temperature rather than entropy. Converting to entropy requires an additional term proportional to ∇C_p, which arises from the derivative of the thermodynamic relation $dS = C_p dT/T$. Far from T_λ, $\nabla\rho_s$ is negligible, and in zero gravity $\nabla\rho_s = 0$ for all ε. In either case the differential equation (6) reduces to the linear form (1).

The temporal and spatial components in the differential equation (6) can be separated for the case of a harmonically driven second-sound resonator using

$$q = \mathrm{Re}[\mathcal{q}e^{i\omega t}] , \tag{7}$$

where ω is the driving frequency and $\mathcal{q}$, complex, is the power input per unit area. In the steady state this power is transmitted through the fluid by a second-sound temperature wave:

$$T_1(z,t) = \mathrm{Re}[\mathcal{T}_1(z)e^{i\omega t}] . \tag{8}$$

Substituting (8) into (6) and eliminating $e^{i\omega t}$ gives

$$-\omega^2\mathcal{T}_1(z) = u_{\mathrm{II}}^2(z)[\nabla^2\mathcal{T}_1(z) + \nabla\rho_s(z)\nabla\mathcal{T}_1(z)/\rho_s] . \tag{9}$$

The solution to (9) requires the definition of boundary conditions at both ends of the resonator. The boundary conditions at a superfluid He/thermal diffusive wall interface have been used to find the exact solution[10] to the homogeneous (zero-gravity, no dissipation) problem [Eq. (1)]. In the MLP experiment, only the heater end of the resonator was a truly solid wall. Their detector consisted of a powdered paramagnetic salt pill, developed by Chui and Marek.[11] These authors show that, in the frequency and temperature regime of MLP, second-sound couples primarily through a thermal diffusive wave to the salt pill. Thus, it appears reasonable to apply thermal diffusive boundary conditions to both ends of the MLP resonator, taking into account the different material parameters.

In order to introduce the many parameters involved, we include a brief derivation from Ref. 10 of the matching boundary equations for the ends of the second-sound resonator, generalizing them for nonzero gravity. The required boundary conditions for He II at a solid wall are given by London:[12]

$$(\rho S v_n - \kappa\nabla T/T)_\perp = q_\perp/T \tag{10}$$

and

$$T = T' - Rq_\perp , \tag{11}$$

where ρ is the He II density, v_n is the velocity of the normal fluid, κ is the thermal conductivity of the normal fluid, T' is the temperature in the wall, and R is the Kapitza boundary resistance.

The normal velocity v_n is related to ∇T through an equation from two-fluid hydrodynamics:[7]

$$dv_n/dt = -(\rho_s/\rho_n)S\nabla T . \tag{12}$$

In the harmonically driven cell the small variations in velocity and temperature are given by

$$v_n = \mathrm{Re}[\mathcal{v}_n(z)e^{i\omega t}] \tag{13}$$

and

$$T = \mathrm{Re}[\mathcal{T}(z)e^{i\omega t}] . \tag{14}$$

Substituting (13) and (14) into (12) and simplifying yields

$$i\omega\mathcal{v}_n = -(\rho_s/\rho_n)S\nabla\mathcal{T} . \tag{15}$$

Eliminating v_n from (10) and (15) gives the boundary condition in terms of $\nabla\mathcal{T}$:

$$(-\rho S^2 T\rho_s/i\omega\rho_n - \kappa)\nabla\mathcal{T} = \mathcal{q} . \tag{16}$$

With a constant amplitude power input, the boundary equation (16) at the heater end of the cell becomes

$$(-\rho S^2 T\rho_s/i\omega\rho_n - \kappa)_0\nabla\mathcal{T}_0 = \mathcal{q}_0 , \tag{17}$$

where the subscript (0) indicates quantities to be evaluated at $z=0$, the boundary between the heater and the fluid. At the detector end of the cell, the power transmitted through the boundary is the heat flux: $\mathcal{q} = -\kappa'\nabla\mathcal{T}'_L$, where κ' is the thermal conductivity in the wall and the subscript L indicates quantities to be evaluated at $z=L$, the interface between the fluid and the detector. Thus, the boundary equation (16) at $z=L$ becomes

$$(-\rho S^2 T\rho_s/i\omega\rho_n - \kappa)_L\nabla\mathcal{T}_L = -\kappa'\nabla\mathcal{T}'_L . \tag{18}$$

Similarly (11) becomes

$$\mathcal{T}_L = \mathcal{T}'_L + R\kappa'\nabla\mathcal{T}'_L . \tag{19}$$

In a solid wall heat travels as a thermal diffusive wave which is given by[13]

$$T' = \mathrm{Re}[\mathcal{T}_b e^{-z'(i-1)/\delta}e^{i\omega t}] , \tag{20}$$

where $\mathcal{T}_b$ is the temperature at the boundary $z'=0$, and the thermal penetration depth δ is given by

$$\delta^2 = 2\kappa'/\rho' C'_p\omega , \tag{21}$$

where ρ' and C'_p are properties of the wall material. For convenience we scale $z' = z - L$ so that

$$\mathcal{T}'_{z=L} \equiv \mathcal{T}_b \tag{22}$$

and

$$\nabla\mathcal{T}'_{z=L} = -\mathcal{T}_b(i-1)/\delta . \tag{23}$$

Substituting (22) and (23) into (18) and (19) yields

$$\alpha_L\nabla\mathcal{T}_L = \kappa'\mathcal{T}_b(i-1)/\delta \tag{24}$$

and

$$\mathcal{T}_L = \mathcal{T}_b[1 - R\kappa'(i-1)/\delta] , \tag{25}$$

where we define

$$\alpha \equiv \alpha_1 + i\alpha_2 = -\kappa + i\rho S^2 T\rho_s/\omega\rho_n . \tag{26}$$

Dividing (24) and (25) gives

$$\alpha_L\nabla\mathcal{T}_L/\mathcal{T}_L = -2\kappa'/[\delta(1+i) + 2R\kappa'] . \tag{27}$$

The differential equation (9) along with the boundary conditions (17) and (27) form the description of the second-sound boundary-value problem for small amplitudes with no damping. For a given driving frequency ω, the equations can be solved numerically using the "shooting method."[14] The ordinary shooting method is easily modified to handle complex quantities. First we decompose the second-order differential equation into first-order equations. By making the following substitutions into (9), $y_1=\mathrm{Re}[\mathcal{T}_1]$, $y_2=\mathrm{Re}[\nabla\mathcal{T}_1]$, $y_3=\mathrm{Im}[\mathcal{T}_1]$, and $y_4=\mathrm{Im}[\nabla\mathcal{T}_1]$, we obtain four coupled first-order differential equations:

$$y_2=\nabla y_1 , \tag{28}$$

$$\omega^2 y_1+u_{\mathrm{II}}^2[\nabla y_2+(\nabla\rho_s/\rho_s)y_2]=0 , \tag{29}$$

$$y_4=\nabla y_3 , \tag{30}$$

$$\omega^2 y_3+u_{\mathrm{II}}^2[\nabla y_4+(\nabla\rho_s/\rho_s)y_4]=0 . \tag{31}$$

The shooting method is initialized by guessing the second-sound amplitude at the bottom of the resonator ($z=0$): $y_1(0)\equiv\mathrm{Re}\mathcal{T}_1(0)$, $y_3(0)\equiv\mathrm{Im}\mathcal{T}_1(0)$. The gradient of temperature at this interface, $y_2(0)\equiv\mathrm{Re}\nabla\mathcal{T}_1(0)$ and $y_4(0)=\mathrm{Im}\nabla\mathcal{T}_1(0)$, is calculated using the boundary condition (17). Equations (28)–(31) are then integrated using, for example, the Runge-Kutta[14] method, giving values for $y_1(z)$ ($i=1,\ldots,4$) along the length of the cell. The deviations of the values $y_i(L)$ from the boundary equation (27) are used to obtain a better estimate of the second-sound amplitude $[y_1(0),y_3(0)]$. The Runge-Kutta method is applied iteratively until the boundary condition at $z=L$ is matched to within a specified tolerance. The resonant frequency is found by maximizing the result of the shooting method, $|\mathcal{T}_1(L)|^2\equiv y_1(L)^2+y_3(L)^2$ as a function of frequency. By using an appropriate choice of the frequency range, the maximization routine can be used to determine the fundamental wave function or any harmonic.

Figure 2 shows the fundamental wave function obtained from maximizing the response at the detector end of the MLP cell. Three curves are plotted for different values of reduced temperature ε at the bottom of the cell; the effective temperature difference from the local T_λ increases by 1.6 μK at the top. For $\varepsilon>10^{-6}$, where gravity effects are small, the wave function is nearly symmetrical as expected from the analytical solution of (1). As the bottom of the cell approaches T_λ, the distortion of the wave function reveals the inhomogeneity of the superfluid. Only the real part of the wave function $[y_1(z)]$ is plotted in Fig. 2; the imaginary part $[y_3(z)]$ is negligible on this scale, indicating the wave function is real on resonance.

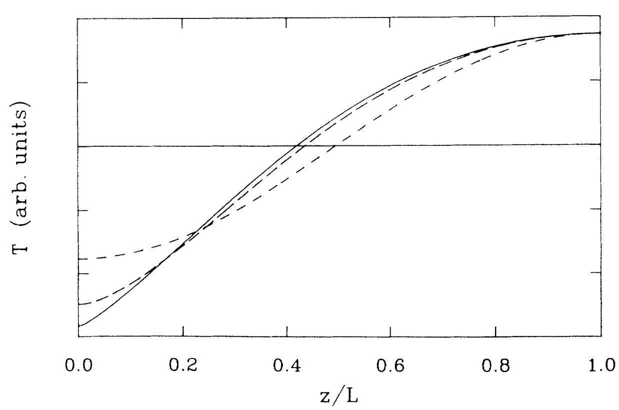

FIG. 2. Temperature wave in second-sound resonator of length L ($=1.3$ cm) at the fundamental frequency, computed for three different temperatures. The solid line corresponds to $\varepsilon=10^{-9}$, the long-dashed line to $\varepsilon=10^{-7}$, and the medium-dashed line to $\varepsilon=10^{-5}$, all referred to the bottom of the cell.

III. HIGHER-ORDER EFFECTS

In this section we consider a number of ways that the above treatment can be extended to give a more realistic representation of experiment. First we consider the effect of second-sound damping. The derivation of the damping term follows from Khalatnikov's superfluid hydrodynamic equations[7] including dissipation:

$$\partial^2 T_1(z,t)/\partial t^2=u_{\mathrm{II}}^2(z)[\nabla^2 T_1(z,t)+\nabla\rho_s(z)\nabla T_1(z,t)/\rho_s] \\ +D_2\nabla^2\partial T_1(z,t)/\partial t , \tag{32}$$

where D_2 is the second-sound damping coefficient. Separating the temporal and spatial components as before gives

$$-\omega^2\mathcal{T}_1(z)=u_{\mathrm{II}}^2(z)[\nabla^2\mathcal{T}_1(z)+\nabla\rho_s(z)\nabla\mathcal{T}_1(z)/\rho_s] \\ -\omega D_2\nabla^2 T_1(z) . \tag{33}$$

To estimate the effects of the damping term alone, we set $\nabla\rho_s=0$ and neglect gravity and finite-amplitude effects. The traveling wave solution to the differential equation is of the form $T_1=T_0e^{ikz-i\omega t}$, with complex wave vector $\mathbf{k}=k_z+i\omega^2D_2/2u_{\mathrm{II}}^3$, where k_z is the wave vector with no dissipation. This solution was also obtained by Putterman[15] through direct substitution into the hydrodynamic equations. It is interesting to see how the dispersion relation ($\omega_0^2=k_z^2u_{\mathrm{II}}^2$) is modified by damping. Substituting the traveling wave solution into (33) and simplifying gives

$$\omega^2=\omega_0^2/[1-(k_zD_2/u_{\mathrm{II}})^2] \\ \approx\omega_0^2[1+(k_zD_2/u_{\mathrm{II}})^2] .$$

The deviation from the ideal case grows as T_λ is approached due to the divergence of both D_2 and u_{II}^{-1}. At $\varepsilon=2\times10^{-5}$, the closest temperature to T_λ at which D_2 has been measured,[16] we find $D_2=8\times10^{-4}$ cm^2/sec and $u_{\mathrm{II}}=79$ cm/sec. With $k_z=2.4$ cm^{-1}, corresponding to the length of the MLP resonator, the fractional frequency shift $(k_zD_2/u_{\mathrm{II}})^2$ is 6×10^{-10}. A rough extrapolation of the experimental results to $\varepsilon=10^{-7}$ gives $D_2\sim6\times10^{-3}$ cm^2/sec and $u_{\mathrm{II}}\sim9$ cm/sec, and a corresponding fractional frequency shift of 3×10^{-6}. In a resonator, the steady-state solution consists of two oppositely directed traveling waves. Because the shift is so minute for a single traveling wave, we expect the damping effect in the resonator to be, at most, a very small perturbation to the undamped case, even when generalized to nonzero gravity. We anticipate that future experimental work will approach closer to T_λ where the damping may become significant. For this reason as well as to verify that damping is negligible in the MLP regime, we show how (28)–(31) are modified to include damping:

$$y_2 = \nabla y_1 , \tag{34}$$

$$\omega^2 y_1 + u_{\rm II}^2[\nabla y_2 + (\nabla\rho_s/\rho_s)y_2] - \omega D_2 \nabla y_4 = 0 , \tag{35}$$

$$y_4 = \nabla y_3 , \tag{36}$$

$$\omega^2 y_3 + u_{\rm II}^2[\nabla y_4 + (\nabla\rho_s/\rho_s)y_4] + \omega D_2 \nabla y_2 = 0 . \tag{37}$$

The numerical techniques for solving this set of equations are the same as before with the solution reducing to the nondamped case when $D_2=0$.

The second nonlinear effect we consider arises from the finite amplitude of the second-sound wave. Putterman and Garrett[17] derive a second-order equation, using the first-order result $T_1(z,t)$ obtained from (6) [or (32) if damping is to be included] as a driving term for a second-order excitation $T_2(z,t)$:

$$\partial^2 T_2(z,t)/\partial t^2 - u_{\rm II}^2(z)\partial^2 T_2(z,t)/\partial z^2 = \gamma(z)\partial^2 T_1^2(z,t)\partial t^2 , \tag{38}$$

where $\gamma \equiv (d/dT)\ln(u_{\rm II}^3 \partial s/\partial t)$ is Khalatnikov's nonlinear coefficient.[7] The subscripts 1 and 2 follow the notation of Ref. 17. An upper bound on the frequency shift due to finite-amplitude effects can be estimated from the shift[17] in the second-sound velocity (u) in a *traveling wave* of amplitude T_1: $u = u_{\rm II0}(1+\gamma T_1)$, where $u_{\rm II0}$ is the velocity at zero amplitude. When the two oppositely directed traveling waves in a resonator are summed, the finite-amplitude shift tends to cancel, thus, $\delta f/f \equiv \delta u/u_{\rm II0} \ll \gamma T_1$. From the results of a least-squares fit to the MLP data discussed later, we obtain $T_1 = 8.1\times10^{-9}$ K at the low end of the fitted range, i.e., $\varepsilon = 2\times10^{-7}$. Using an effective $\gamma = 1.4\times10^6$ averaged over the length of the cell gives a frequency shift due to finite-amplitude effects of $\delta f/f \ll 1.1\%$. For $\varepsilon \geq 2\times10^{-7}$ we expect that the cancellation reduces the shift to $<0.2\%$, much smaller than the scatter in the MLP data. However, it is possible that this effect may slightly perturb the parameters derived from the data.

In cases where the second-order amplitude T_2 is significant, other second-order, or even third-order, effects may also be important. Recently, Goldner, Ahlers, and Mehrotra[18] (GAM) described an experimental method for extracting the superfluid fraction near T_λ from an analysis of highly nonlinear second-sound pulses reflecting between a heater and bolometer. Although the experimental temperature range examined by GAM (2–25 mK) is further from T_λ than the present work, GAM anticipate that their method will be useful very near T_λ where they expect nonlinear effects to be important. For the work closer to T_λ, GAM point out that an analysis of the self-interactions of the pulses upon reflection as well as coupling to first sound may need to be carried out. A thorough analysis would include $\nabla\rho_s$ terms in the differential equation and estimate the effects of third-order terms, similar to our estimating second-order effects in this work. GAM state that the pulse method should be more effective very near T_λ as it does not depend on the linearity of second sound which breaks down sufficiently close to T_λ. However, our analysis in the next section indicates that, in the MLP experiment, amplitude nonlinearities were essentially negligible to $\varepsilon \sim 10^{-7}$. The ability to reduce the amplitude of the sound to the linear region greatly simplifies the overall analysis.

A more quantitative analysis of the finite-amplitude effects in our model is obtained from the solution of (9) and (38). The gravitational effects are incorporated into the finite-amplitude problem by allowing γ and $u_{\rm II}$ in (38) to vary with height. The calculation of the finite-amplitude effects closely follows the numerical solution described in the previous section. The differential equation (38) is driven by the square of the first-order temperature wave $T_1(z,t)$. From the square of (8) we see that the second-order amplitude $T_2(z,t)$ oscillates at frequency 2ω in the steady state. Thus, the thermal diffusive boundary conditions (20) and (21) must be modified for penetration of a wave at frequency 2ω. In contrast with the first-order wave, thermal diffusive boundary conditions apply at *both* ends of the resonator for the second-order temperature wave. The driving power q_0 oscillating at frequency ω does *not* couple directly to T_2, which oscillates at 2ω.

Separation of the spatial and temporal variables in (38) yields

$$4\omega^2 \mathcal{T}_2(z) + u_{\rm II}^2(z)\nabla^2\mathcal{T}_2(z) = 4\omega^2\gamma(z)\mathcal{T}_1^2(z) . \tag{39}$$

To be self-consistent, (39) and (9) are solved simultaneously. This is accomplished in the shooting method by introducing four parameters $y_5 = \mathrm{Re}[\mathcal{T}_2]$, $y_6 = \mathrm{Re}[\nabla\mathcal{T}_2]$, $y_7 = \mathrm{Im}[\mathcal{T}_2]$, and $y_8 = \mathrm{Im}[\nabla\mathcal{T}_2]$. There are now eight coupled first-order differential equations, (28)–(31), and the following:

$$y_6 = \nabla y_5 , \tag{40}$$

$$4\omega^2 y_5 + u_{\rm II}^2 \nabla y_6 - 4\omega\gamma(y_1^2 - y_3^2) = 0 , \tag{41}$$

$$y_8 = \nabla y_7 , \tag{42}$$

$$4\omega^2 y_7 + u_{\rm II}^2 \nabla y_8 - 8\omega\gamma y_1 y_3 = 0 . \tag{43}$$

The resonant frequency solution is obtained numerically as before. A corresponding plot to Fig. 2 with finite-amplitude effects included is beyond the scope of this work as a third dimension for amplitude is required. For small enough amplitudes this graph would reduce to Fig. 2.

In the next section we describe the results of fitting our model to the MLP data, initially neglecting second-sound damping and finite-amplitude effects. We then show the significance of the additional nonlinear effects.

IV. RESULTS AND DISCUSSION

The numerical determination of a resonant wave function represents a fitting function whose output is the resonant frequency ω, containing seven free parameters: ζ, k_0, k_1, a_0, ΔT_λ, $\delta/2\kappa'$, and R. As the MLP data did not lend itself to obtaining an accurate estimate of the parameters k_1 and a_0, we used the previously published values[5] $k_1=-1.47$ and $a_0=0.32$. We reduced the number of free parameters further by noting that the results of the fit were insensitive to the value of both $\delta/2\kappa'$ and R. Thus, we fixed these parameters at the estimated values obtained from Ref. 19: $\delta/2\kappa'=6.76\times10^{-7}$ cm^2 K$\sqrt{\mathrm{Hz}}$/W and $r=0.5$ cm^2 K/W. Figure 3 shows the deviation of the MLP data from a least-squares fit to our model (with $D_2=0$ and neglecting finite amplitudes), containing the remaining free parameters: ζ, k_0, and ΔT_λ. The range of the fit extended from $\varepsilon=10^{-3}$ down to $\varepsilon=2\times10^{-7}$. The lower limit was chosen as the point where the amplitude $T_1(0)$ at the bottom of the cell was 2% of the distance to T_λ of the local time-averaged cell temperature T, i.e., $T_1(0)=0.02\times\varepsilon(0)T_\lambda$. It should be noted that this cutoff point is somewhat less than the "gravity limit" $\varepsilon=3.8\times10^{-7}$, which marks the point at which gravity effects become significant. In principle, there is no reason why a smaller cutoff could not be used, by many of the approximations in the present model will soon break down, as discussed below.

The best-fit values for ζ and k_0 are given in Table I, along with previous theoretical and experimental results. Our result for ζ agrees with the Greywall-Ahlers (GA) result[5] and the RG prediction to within one standard deviation uncertainty. It is interesting to note that the associated value of α' obtained on the basis of scaling is $\alpha'=-0.0124\pm0.002$, close to the observed value[8] over a similar temperature range, and in reasonable agreement with either of the RG predictions:[4] $\alpha'=-0.0066$ or -0.016. The uncertainty in k_0 partially reflects the uncertainty in the length of the MLP resonator due to the porous salt pill detector. The third parameter in our model, ΔT_λ, has a best-fit value of $1.486\times10^{-7}\pm0.344\times10^{-7}$ K. We found that the introduction of this parameter was crucial in obtaining a good fit. If MLP had included a shift in T_λ from the raw data, it is possible their fit could have been extended to smaller ε. To test this hypothesis, we modified our model to closely approximate the time-of-flight model: the term proportional to $\nabla\rho_s$ in (9) was eliminated and the detector boundary parameters were replaced by those of glass, a more insulating boundary. The results shown in Fig. 4, of a least-squares fit using this simplified model, improve upon the MLP deviations to $\varepsilon\sim10^{-6}$. This indicates that the $\nabla\rho_s$ term and the boundary effects included in our model are significant. Thus, the time-of-flight model is probably not accurate below $\varepsilon\sim10^{-6}$. We have also investigated the effect of setting ΔT_λ in our model to zero. The results plotted in Fig. 5 show deviations slightly larger than MPL using the time-of-flight model, see Ref. 6. It is thus obvious that the improved model alone cannot explain the MLP results.

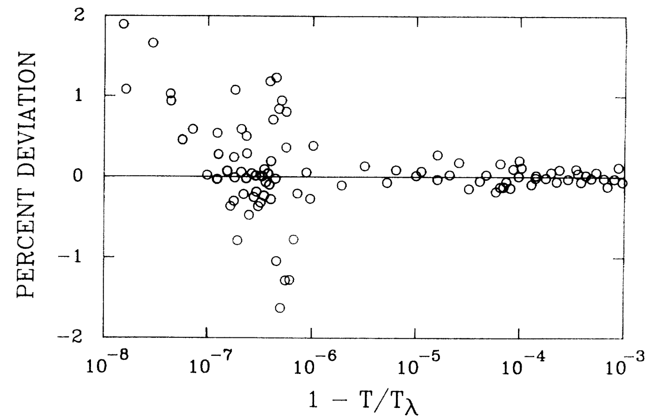

FIG. 3. Deviations of the second-sound frequency from a least-squares fit to the model described in the text. The reduced temperature of the raw data has been shifted by the value of the fitted parameter ΔT_λ.

The satisfactory results of the fit to our model in Fig 3, which neglects second-sound damping and finite amplitudes, indicates that these effects are indeed small. To confirm that second-sound damping is negligible in the MLP experiment, we performed a least-squares fit with nonzero D_2 in (33), but neglecting finite amplitudes. The existing experimental data[16] for the damping coefficient only cover the range $\varepsilon>2\times10^{-5}$, necessitating extrapolation of the results to smaller ε. The deviations in the fitted parameters from the undamped case were less than 0.01%, much less than the estimated uncertainty in the parameters. These results are in agreement with the discussions in Sec. III.

To confirm that finite-amplitude effects are negligible over the range of our fit, we computed the resonant frequency using our finite-amplitude model at the lower limit $\varepsilon=2\times10^{-7}$. The deviation of the frequency from the results of our best fit (Fig. 3) is less than 0.05% at the low end of the reduced temperature range and decreased with increasing ε. As this is much less than the scatter in the MLP data, we expect no effect of finite amplitude on our

TABLE I. Summary of recent experimental and theoretical results for the scaling parameter ζ and the amplitude k_0 along with the range of data examined.

	ζ	k_0	Range of fit
RG	0.672 ± 0.002		
Present work	0.6708 ± 0.0004	2.502 ± 0.007	$2\times10^{-7}<\varepsilon<10^{-3}$
MLP	0.6740 ± 0.0005	Scaled to GA value	$10^{-6}<\varepsilon<10^{-3}$
GA	0.6716 ± 0.0004	2.467[a]	$2\times10^{-5}<\varepsilon<10^{-2}$

[a]There is no uncertainty given for this value in Ref. 5.

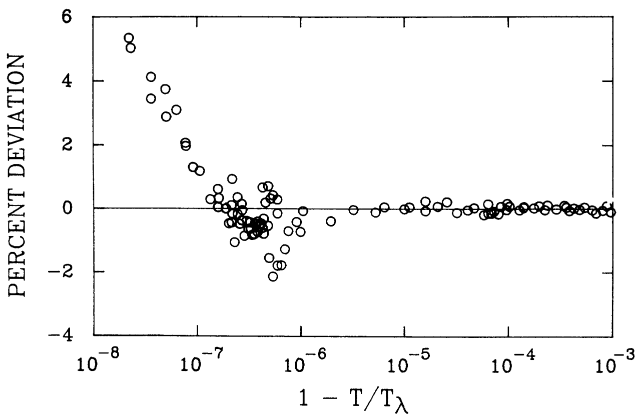

FIG. 4. Deviations of the second-sound frequency from a least-squares fit to the model which has been modified to approximate the MLP time-of-flight model but includes a shift in T_λ.

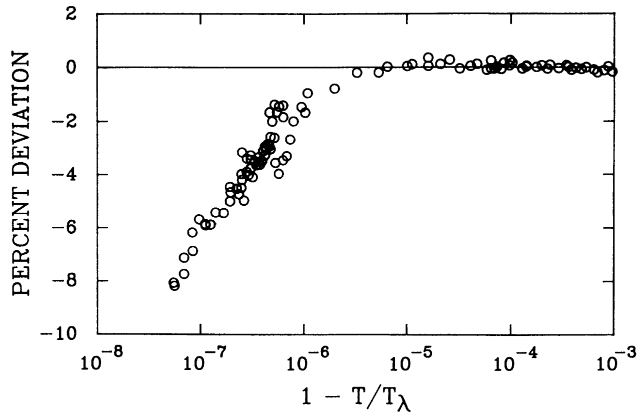

FIG. 5. Deviation of the second-sound frequency from a least-squares fit over the range $1.2\times10^{-7}<\varepsilon<1\times10^{-3}$ with ΔT_λ fixed at 10^{-10} K.

fitted parameters. We also found that the second-order amplitude T_2 is 3 orders of magnitude less than the first-order amplitude T_1, consistent with the approximation $T_2 \ll T_1$ used in deriving the differential equation for T_2.

At first sight the magnitude of the shift in T_λ from the MLP estimate is troubling, considering that the sensitivity of their thermometers was 2 orders of magnitude higher. Furthermore, the value of the shift places two data points above T_λ, although by less than the uncertainty of the shift. However, it is possible to reinterpret the MLP data used to estimate T_λ in a way that agrees with our estimate of T_λ. The MLP estimate is based on two different methods. The first method, observation of an abrupt change in thermal conductivity of the cell as the temperature is swept through T_λ, had an uncertainty of about $\pm10^{-7}$ K. The second method, a linear *extrapolation* of the second-sound amplitude to zero as T_λ is approached, had an uncertainty of $\pm3\times10^{-8}$ K and is consistent with the first method. Since the amplitude extrapolation is the most important, it is worth considering in detail what the temperature dependence of the amplitude might be. Using the model described above, we have calculated the amplitude of the second-sound wave as a function of ε. For constant driving power, the amplitude is 1×10^{-9} K at $\varepsilon=10^{-3}$, rising smoothly to 8.1×10^{-9} K at $\varepsilon=2\times10^{-7}$. Extrapolating this trend closer to T_λ, one finds that the positive temperature swing of the second-sound wave will approach arbitrarily close to T_λ for $\varepsilon\sim10^{-8}$. Beyond this point the amplitude should be reduced due to second-sound damping and/or finite-amplitude effects which convert energy from the fundamental frequency to generate higher harmonics. We believe this effect would lead to a sharp drop-off in amplitude, yielding a much steeper slope than assumed by MLP. Thus, the lowest-frequency MLP data could be essentially at T_λ in agreement with our estimate.

It is instructive to review some of the approximations in our model which may lead to systematic errors in the fit. When the positive temperature swing of the second-sound wave approaches T_λ, additional damping and/or finite-amplitude effects will take energy out of the wave, suppressing the amplitude. This manifestation of second-sound damping and finite-amplitude effects is not tenable with our model. Furthermore, to properly calculate the wave function in this situation, even while neglecting damping and finite amplitudes, would entail the insertion of time dependence into $u_{\rm II}(z)$ and $\nabla\rho_s(z)$, e.g., $u_{\rm II}(z,t)\equiv u_{\rm II}[\varepsilon(z,t)]$, where

$$\varepsilon(z,t)=\{T_\lambda(z)-T-\mathrm{Re}[\mathcal{T}(z)e^{i\omega t})]\}/T_\lambda(z)\ .$$

Solving this problem requires more sophisticated numerical techniques as the time and spatial variables are no longer separable as in (9).

We have made several other approximations which are expected to break down sufficiently close to T_λ. First, the hydrodynamic equations take on a different form[7,19] with ρ_s treated as a fifth independent parameter. In this treatment an additional parameter is introduced describing the relaxation of ρ_s toward equilibrium. Second, interactions between layers of different superfluid density invalidate the approximation (see Sec. II) that the local properties of ^{4}He are given by the locally homogeneous fluid.[20] Third, the finite power dissipated in the heater may lead to a detectable depression of T_λ.[21] A clear cutoff is not known for when these effects become important. However, the agreement of our model with the experimental data is strong evidence for the validity of our approach using superfluid hydrodynamics to within $\varepsilon\sim10^{-7}$. An approximation which does not fail near T_λ, but may contribute to uncertainties in the fitted parameters, is the modeling of the detector interface as a thermal diffusive boundary. This is a first-order approximation which ignores coupling to fourth sound and lumps the parameters (κ',δ,R) of the salt grains and ^{4}He together (see Sec. II and Ref. 11).

V. CONCLUSION

We have developed a numerical method for solving the boundary value problem of second sound in a resonant cavity under the influence of the gravitational inhomogeneity. The model was extended to include second-sound damping and finite-amplitude effects. Application of this model to existing second-sound data, combined with a shift in the location of T_λ, allows satisfactory agreement with RG predictions for the critical exponent ζ. The agreement is extended over the entire range of the data. Neither the new model or the T_λ shift alone are sufficient to obtain a good fit to the data. The results indicate that second-sound damping and finite-amplitude effects are negligible in the regime of the MLP experiment except extremely close to T_λ where the amplitude of the wave itself approaches T_λ on the positive temperature swing. Our model overcomes many of the limitations of the MLP time-of-flight model and represents a significant improvement in the treatment of gravitational effects in superfluid helium. In particular, we show that the variations in superfluid density due to gravity have an important effect on the propagation of second sound for $\varepsilon < 10^{-6}$. Future second-sound experiments should strive for a more accurate determination of the transition temperature. In addition, the range of useful measurements could be pushed closer to T_λ with a shorter cell and a reduction in the driving amplitude.

ACKNOWLEDGMENTS

We thank A. L. Fetter, K. W. Rigby, and J. Nissen for helpful discussions. This work was supported by NASA Contract No. 957448.

---

[1] J. A. Lipa, B. C. Leslie, and T. C. Wallstrom, Physicia B **107**, 131 (1981); V. Steinberg and G. Ahlers, J. Low. Temp. Phys. **53**, 255 (1983); T. C. P. Chui and J. A. Lipa, *Proceedings of the 17th International Conference on Low Temperature Physics, LT-17, Karlsruhe, 1984* (North-Holland, Amsterdam, 1984), p. 931; G. K. S. Wong, P. A. Crowell, H. A. Cho, and J. D. Reppy, Phys. Rev. Lett. **65**, 2410 (1990).

[2] G. Ahlers, Phys. Rev. **171**, 275 (1968).

[3] D. Marek, J. A. Lipa, and D. Philips, Phys. Rev. B **38**, 4465 (1988).

[4] D. Z. Albert, Phys. Rev. B **25**, 4810 (1982); J. C. LeGuillou and J. Zinn-Justin, *ibid.* **21**, 3976 (1980).

[5] G. Ahlers, Physica B **107**, 347 (1981); D. S. Greywall and G. Ahlers, Phys. Rev. A **7**, 2145 (1973).

[6] Although there is little physical significance in the results of a least-squares fit which does not fit the data, we report the optimum parameters here for reference. From the fit which neglects $\nabla\rho_s$ terms we obtain $\zeta = 0.6717 \pm 0.0004$, $k_0 = 2.5201 \pm 0.0009$, and $\Delta T_\lambda = 74.7 \pm 24.2$ nK. From the fit using our model alone, with no shift in T_λ, we obtain $\zeta = 0.6724 \pm 0.0004$ and $k_0 = 2.5354 \pm 0.0008$.

[7] I. M. Khalatnikov, *An Introduction to the Theory of Superfluidity* (Benjamin, New York, 1965).

[8] J. A. Lipa and T. C. P. Chui, Phys. Rev. Lett. **51**, 2291 (1983).

[9] T. C. P. Chui and D. R. Swanson, Physica B **165&166**, 565 (1990).

[10] D. R. Swanson, T. C. P. Chui, K. W. Rigby, and J. A. Lipa, Physica B **165&166**, 561 (1990).

[11] T. C. P. Chui and D. Marek, J. Low. Temp. Phys. **73**, 161 (1988).

[12] F. London, *Superfluids* (Wiley, London, 1954), Chap. 19.

[13] H. S. Carslaw and J. C. Jaeger, *Conduction of Heat in Solids*, 2nd ed. (Clarendon, Oxford, 1959).

[14] For discussion and further references on numerical methods we refer the reader to W. H. Press, B. P. Blannery, S. A. Teukolsky, and W. T. Vetterling, *The Art of Scientific Computing* (Cambridge University Press, Cambridge, 1986).

[15] S. J. Putterman, *Superfluid Hydrodynamics* (North-Holland/American Elsevier, Amsterdam, 1974), Sec. 25.

[16] R. Mehrotra and G. Ahlers, Phys. Rev. Lett. **51**, 2116 (1983); Phys. Rev. B **30**, 5116 (1984).

[17] S. Putterman and S. Garrett, J. Low Temp. Phys. **27**, 543 (1977).

[18] L. S. Goldner, G. Ahlers, and R. Mehrotra, Phys. Rev. B **43**, 12 861 (1991).

[19] L. P. Pitavskii, Zh. Eksp. Teor. Fiz. **35**, 408 (1958) [Sov. Phys. JETP **8**, 282 (1959)]; I. M. Khalatnikov, *ibid.* **57**, 489 (1969) [**30**, 268 (1970)].

[20] J. V. Sengers and J. M. J. van Leeuwen, Int. J. Thermophys. **6**, 545 (1985).

[21] G. Ahlers and R. V. Duncan, *Proceedings of the Landau Memorial Conference on Frontiers of Physics* (Pergamon, New York, 1988), p. 219.